2024 NA62 Status Report to the CERN SPSC

NA62 Collaboration

April 2024

Abstract

The status of the NA62 experiment is reported. The 2023 data taking, the hardware and software activities, and the plans for 2024 are discussed. The $K^+ \to \pi^+ \nu\bar{\nu}$ analysis of the 2021-2022 data is presented, together with the highlights of rare and forbidden decay analyses and searches for exotic processes.

CERN-SPSC-2024-012 / SPSC-SR-345
23/04/2024

Contents

1 Introduction

After the completion of data taking in 2016–2018 (RUN1) and obtaining the first $> 3\sigma$ evidence for the $K^+ \to \pi^+\nu\bar{\nu}$ decay [1], NA62 restarted operations in 2021, took data in 2022 and 2023, and is approved to run until LS3 (RUN2) [2].

Since the previous report in April 2023 [3] NA62 has taken data in 2023 for about 150 days with a very good quality of the spill. During the run the beam intensity were varied to identify the conditions maximizing the $K^+ \to \pi^+\nu\bar{\nu}$ sensitivity. The optimal condition was found at 3/4 of the full beam intensity, a value that was kept fixed from mid-August to the end of the run. The high efficiency of beam delivery of the SPS and of the data acquisition allowed NA62 to collect in 2023 the same amount of bursts as in 2022, despite the shorter period of run. The experiment took advantage from the Cherenkov kaon tagger (KTAG) using H_2 as a radiator instead of N_2, and from the new L0 trigger processor board (L0TP+). All the other sub-detectors worked smoothly except the station 0 of the Gigatracker (GTK0), which had 2 out of 10 chips missing since July to the end of the data taking. NA62 also took 10 days of data in dump configuration at the end of July, with a beam intensity 1.5 times higher than in kaon running.

The 2023 data have been processed online and the data quality fully assessed. The reprocessing with the full calibration constants is ongoing. Preliminary indications suggest that the fraction of bad bursts is 10% or below, at least a factor of 2 lower than in 2022.

The analysis of the $K^+ \to \pi^+\nu\bar{\nu}$ (PNN analysis) of the data collected in 2021 and 2022 is close to completion. Some studies are ongoing to understand the differences with respect to the RUN1 data. The analysis of RUN1 data has led to the publications of new measurements of the $K^+ \to \pi^+\gamma\gamma$ and $K^+ \to \pi^0 e^+\nu\gamma$ decays, and to the preliminary result of the study of the $\pi^0 \to e^+e^-$ decay. New searches of exotics particles produced in K^+ decays have been published. NA62 has also delivered a proof of principle of a possible neutrino tagging technique. The analysis of the dataset taken in 2021 in the beam dump configuration has led to the first searches for feebly interacting particles decaying to di-lepton and hadronic final states. Several analyses using RUN1 data are progressing, with results expected in 2024 both in the context of precision physics and direct searches.

Continuous work is ongoing to keep the offline and online software up to date with the latest CERN-IT requirements. The Monte Carlo production is continuing and more sophisticated biasing methods are being developed to generate significant amounts of rare processes.

After a 2023 YETS dedicated to detector maintenance and to address the GTK0 problems, NA62 has restarted data taking in April 2024. A new FPGA-based TDC FELIX readout board has replaced the TEL62 board to readout the CHANTI detector. The 2024 run is expected to be more than one month longer than the 2023 one, thanks to the extension of the run approved in April 2024. The baseline option is to run at 3/4 of the full beam intensity. A period in beam dump mode like in 2023 is foreseen, and also a week at $< 2\%$ of full intensity to perform ultra-precise measurements within the context of CKM unitarity studies.

The document is organised as follows: Section 2 summarises the 2023 run; Section 3 detail the main hardware activities that took place during the winter shutdown and the plans for the 2024 run; Section 4 describes the data quality monitor and reports about the status of the reprocessing of the 2023 data; the status of the software, computing and simulation is described in Section 5; the $K^+ \to \pi^+\nu\bar{\nu}$ analysis is reported in Section 6; Sections 7, 8 and 9 summarise the status of the analyses of the kaon decays, the neutrino tagging technique and exotic processes, respectively; Section 10 lists the NA62 journal publications from May 2023 till April 2024.

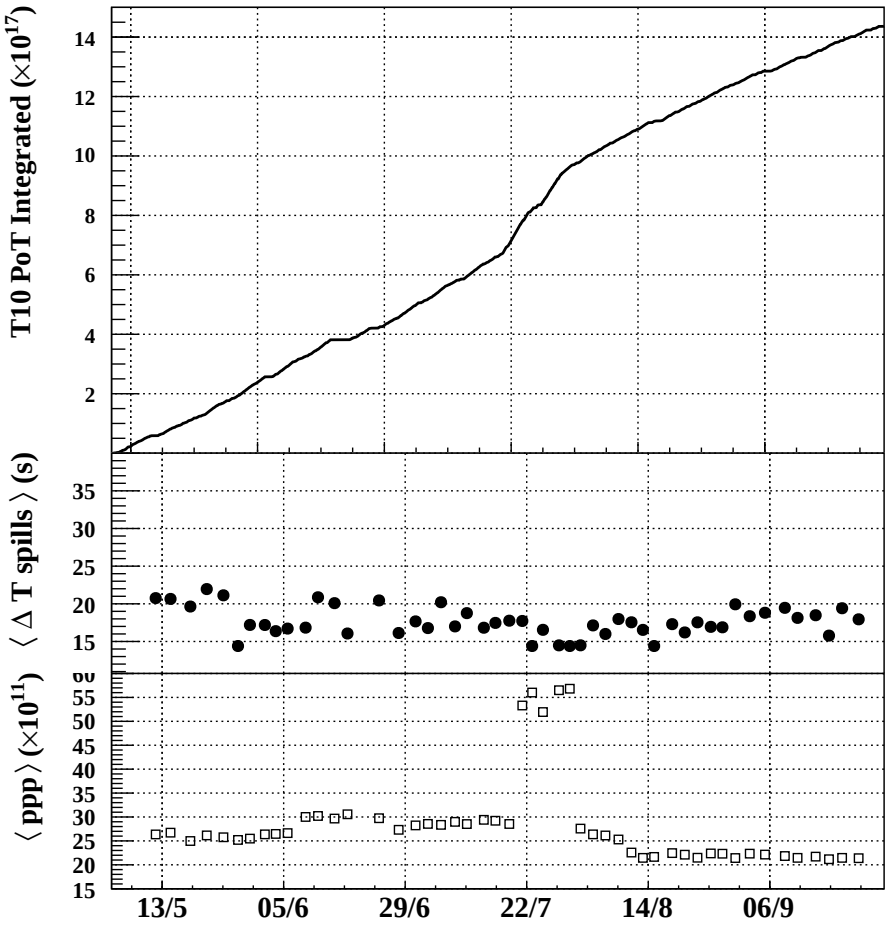

Figure 1: Characteristics of the beam delivered by the SPS to the T10 target in 2023 as a function of the time. Top: integrated protons on target. Middle: time interval between two consecutive spills averaged over about 10^4 spills. Bottom: intensity measured in proton-per-pulse from the T10 intensity monitor averaged over about 10^4 spills. Data reconstructed from TIMBER.

2 2023 Run

NA62 took data in 2023 for 140 days in kaon mode with the standard trigger configuration for $K^+ \to \pi^+\nu\bar{\nu}$ and rare decays, and for 10 days in beam dump mode.

The main changes to the hardware of the experiment in 2023 concerned KTAG, in which the N_2 radiator gas was replaced by H_2, and the L0 trigger processor which made use of the L0TP+ board replacing the previous one (L0TP).

The beam setup was completed successfully before the official start of the data taking. The first week of run was dedicated to commissioning the CEDAR-H. The L0TP+ was operating since the first day, but required some weeks for commissioning, leading to a initial period of reduced data taking efficiency.

From the beginning of June to mid-August NA62 took data at different beam intensities, varying the number of protons on target to find the optimal running conditions to maximize the $K^+ \to \pi^+\nu\bar{\nu}$ yield. A period of run at 3/4 of the full beam intensity followed, in which NA62 collected a sample of data large enough to study the scaling of the backgrounds with intensity.

Table 1: Summary of the 2023 data taking compared to previous years. Columns 2 to 5 are the T4 and T10 availability, the NA62 availability, and DAQ efficiency. The last column is the product of the entries of columns 2 to 5.

Period	T4	T10	NA62	DAQ	Total
2023	0.81	0.96	0.84	0.93	0.61
2022	0.75	0.91	0.84	0.86	0.49
2021	0.71	0.87	0.80	0.73	0.36

2.1 Beam

Following the beam tuning of the P42 and K12 lines, the run restarted on May 10th. The SPS worked smoothly for the whole data taking and delivered an optimal beam quality. The beam quality profited from the removal of the vacuum chamber downstream of the T4 target, that was found significantly misaligned during a beam survey in February 2023. This allowed for a better transmission of the P42 beamline compared to 2022 and for a better focusing of the beam on the T10 target. The fraction of kaons produced per proton on target was higher than in 2022. This led to measuring in the detectors the same particle rate as in 2022 with 30×10^{11} protons on T10 target per pulse (ppp) instead of 33×10^{11}. This intensity corresponded to 60×10^{11} ppp on the T4 target, a value 20% lower than in 2022. In the following 30×10^{11} ppp is taken as the reference for full beam intensity.

In total, in 2023 the SPS delivered 1.44×10^{18} protons on T10 target (PoT)(Fig. 1, top), of which 1.17×10^{18} in kaon mode and 0.27×10^{18} in dump. The average time difference between two consecutive bursts was about 17.6 s. The actual time difference varied during the run from 14.4 s to 20–25 s, depending on the activities in parallel to the SFTPRO cycle (Fig. 1, middle). The intensity on T10 varied from 20×10^{11} ppp to 30×10^{11} (Figure 1, bottom). The beam intensity was increased to 56×10^{11} ppp during the dump. Fluctuations of the order of 10% of the T10 intensity were observed on a daily basis.

2.2 Data taking performance

Table 1 summarizes the 2023 data taking performance obtained from an analysis of the SPS spills recorded by the NA62 run control. The T4 availability is the fraction of spills recorded with beam on T4 with respect to the expected number of spills. The T10 availability is the fraction of spills recorded with beam on T10 and T4 with respect to the spills with beam on T4, and quantifies the amounts of issues with the beam line and the NA62 detectors that required access to ECN3. The NA62 availability is the fraction of spills written on disk compared to the spills recorded with T10 and T4 on. In this case missing spills are due to hardware problems being fixed without stopping the beam on T10. The DAQ efficiency is the fraction of spills recorded by NA62 with a number of triggers consistent with what expected from the intensity. This fraction accounts for possible issues of the online data flow. The product of the NA62 availability and DAQ efficiency is a figure of merit for the NA62 data taking efficiency, which amounted to about 78% in 2023, compared to 72% in 2022. The last column in Table 1 is the product of the previous efficiencies and quantifies the fraction of the data taking period in which NA62 wrote data on disk.

The excellent performance of 2023 stem from a higher data taking efficiency of NA62 and a higher efficiency of beam delivery from SPS, and allowed NA62 to record about 400K bursts in

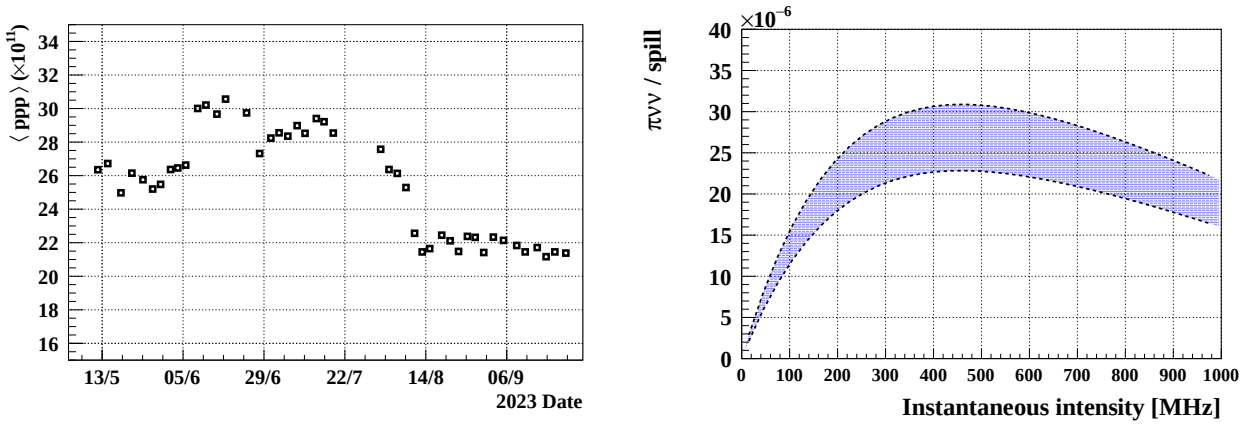

Figure 2: Left: intensity measured in proton-per-pulse from the T10 intensity monitor averaged over about 10^4 spills; data reconstructed from TIMBER. Right: expected number of selected $K^+ \to \pi^+\nu\bar{\nu}$ per spill as a function of the instantaneous intensity.

kaon mode, the same amount as in 2022 despite the shorter run.

2.3 Intensity scan

The beam intensity profile of the data taken in kaon mode is shown in Fig. 2 (left panel). In this plot the intensity is measured burst by burst by a beam monitor and is expressed in terms of protons on target per pulse. This quantity is denoted $\mathcal{A}$ in the following. Each point of Fig. 2 is the average over 10^4 bursts. By definition, $\mathcal{A}$ depends on the actual length of the burst. For example, spills truncated because of extraction problems have lower intensity.

The instantaneous intensity, $\mathcal{I}$, is a quantity measured event by event from the out-of-time activity of the Gigatracker detector and is expressed in MHz. Because of the inter-spill fluctuations of the beam, $\mathcal{I}$ is subject to higher fluctuations than $\mathcal{A}$. The value of $\mathcal{I}$ averaged over a burst, $\langle\mathcal{I}\rangle$, depends on $\mathcal{A}$, but encodes also the information of the beam quality. The full intensity of a spill with optimal beam quality corresponds to about $\langle\mathcal{I}\rangle = 600$ MHz.

The yield of selected $K^+ \to \pi^+\nu\bar{\nu}$ decays as a function of $\mathcal{I}$ is the relevant figure of merit to establish the optimal intensity. The measurement of this yield proceeded with the recording per each burst of the number of $K^+ \to \pi^+\pi^0$ events, $n_{\pi\pi}$, selected using the criteria of the PNN analysis in which $K^+ \to \pi^+\pi^0$ decays are used for normalization. On average, these events are about 400-500 per burst and share with the $K^+ \to \pi^+\nu\bar{\nu}$ decays all the trigger and selection criteria, except the conditions on photon rejection and the definition of the kinematic region. Therefore, sources of inefficiency like trigger, DAQ, detectors and selection affect $n_{\pi\pi}$ similarly to the signal.

A two-dimensional unbinned fit of $n_{\pi\pi}$ as a function of $\mathcal{A}$ and $\langle\mathcal{I}\rangle$ was performed using a paralyzable dead-time model to describe the dependence on $\langle\mathcal{I}\rangle$ of the expected number of selected $K^+ \to \pi^+\pi^0$ decays per burst. A data-driven approach was used to build the probability density function of $\langle\mathcal{I}\rangle$ given $\mathcal{A}$.

The dependence of the signal yield on $\mathcal{I}$ stems from the dependence of $n_{\pi\pi}$ on $\langle\mathcal{I}\rangle$ convoluted with the probability to randomly loose $K^+ \to \pi^+\nu\bar{\nu}$ decays because of the photon rejection conditions. This probability, also called random veto inefficiency, is measured on data using $K^+ \to \mu^+\nu$ decays.

The measured yield is shown in Fig. 2 (right panel) and is expressed in terms of expected

average number of $K^+ \to \pi^+\nu\bar{\nu}$ selected per spill. The curve is the average of the results obtained repeating the fit on different datasets taken all along the run. The spread is due to the uncertainties of the fit parameters that include the fluctuations of the result between datasets, the statistical uncertainty from the fit, and the systematics of the model. The first contribution is the most relevant and is dominated by issues with calibration and reconstruction affecting the online processing of the data.

Data show a broad maximum around 450 MHz, which roughly corresponds to 3/4 of the full intensity. This has been chosen as working point for the rest of data taking, leading to run at an intensity of $(22 \div 23) \times 10^{11}$ ppp instead of 30×10^{11} ppp from mid-August onwards.

3 Status of the hardware and plans for the 2024 Run

3.1 KTAG

The KTAG received a major upgrade in 2023: the N_2 radiator gas was replaced by H_2, thereby reducing the thickness of matter traversed by the beam from 3.9% to 0.7% of a radiation length to decrease scattering and improve beam transmission. A new gas vessel and optics, named CEDAR-H, were built at CERN in 2021, and characterised in a dedicated test-beam at CERN in October 2022. The CEDAR-H replaced the N_2-based setup (CEDAR-W) in the NA62 beam line in March 2023, and has operated successfully during the entire 2023 data taking period. The test-beam results and KTAG performance with H_2 radiator gas in NA62 have been reported in a technical paper in the JINST journal [4].

The CEDAR-H performance in the NA62 conditions was assessed using data collected in 2023, and compared to that of CEDAR-W using data collected in 2022. A sample of charged kaons is obtained from $K^+ \to \pi^+\pi^+\pi^-$ decays reconstructed in the STRAW spectrometer. The KTAG light yield and time resolution are measured using kaon candidates with signals in at least 5 sectors (out of 8), which is the standard kaon tagging requirement. The light yield extracted from the distribution of the number of photoelectrons per kaon candidate (Fig. 3, left) is found to be 20.6 photoelectrons per kaon candidate for CEDAR-H, an improvement over 18.1 photoelectrons achieved with CEDAR-W in 2022. The CEDAR-H time resolution is computed to be 66 ps (compared to 71 ps for CEDAR-W) based on the number of photoelectrons per kaon candidate and the nominal KTAG PMT single-photoelectron time resolution of 300 ps. The K^+ identification efficiency based on 5-fold coincidences is found to be 99.7%, compared to 99.5% for CEDAR-W. The measured efficiency of the two detectors agrees with the analytical expectations based on the observed light yield for (Fig. 3, right).

3.2 GTK

Detector operation was smooth at the beginning of the run until June 5, when two out of ten chips of the first GTK module, station 0, stopped communicating with the corresponding readout boards. Chips could not be recovered with the standard procedures, various tests performed indicated that the problem was related to the GTK module itself. It was exchanged for a new GTK during the next machine development stop.

The same problem appeared on July 13 on the new module at station 0, affecting the same two chips. This module was not replaced during the run, and the two problematic chips were masked until the end of the run.

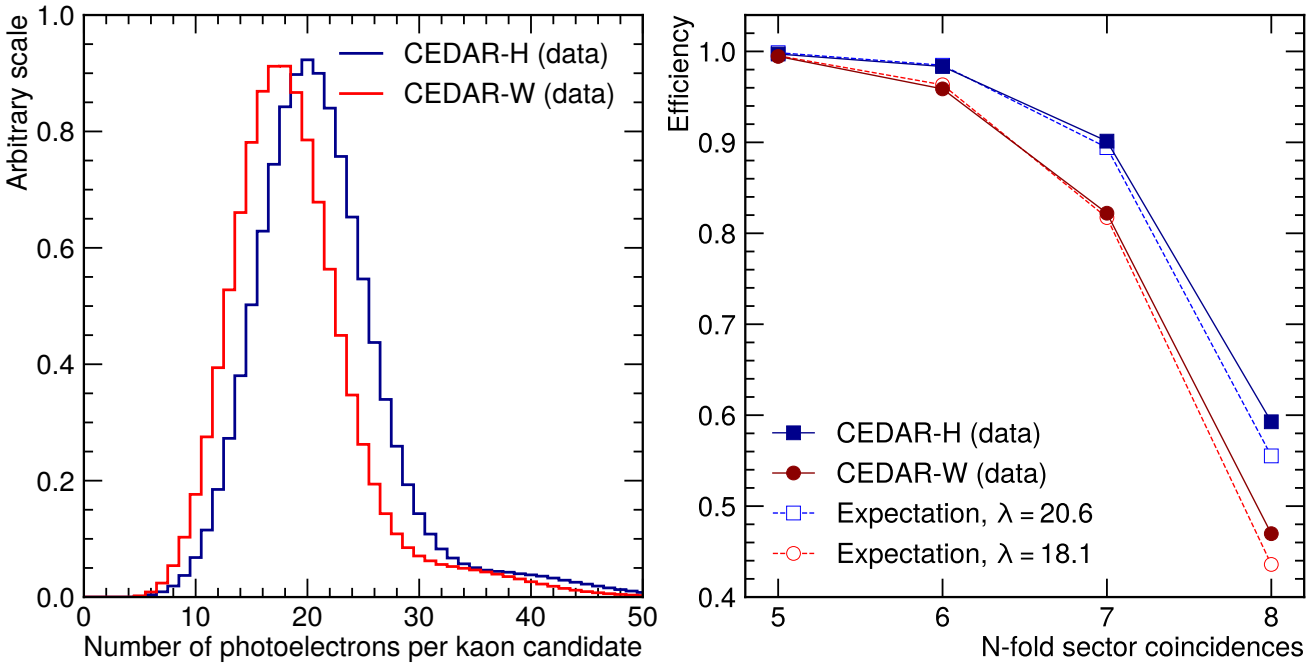

Figure 3: Left: number of photoelectrons per kaon candidate for CEDAR-W and CEDAR-H in the data, reconstructed with a 2 ns time window and normalised to the same integral. Right: K^+ identification efficiency for CEDAR-W and CEDAR-H as a function of N-fold sector coincidences, with analytical expectations for the efficiency given the Poisson mean numbers of photoelectrons of 20.6 and 18.1 from fits to the distributions in the left panel.

Investigation of the problem continued in the lab with the first non-working GTK module. However, the results were inconclusive apart from indicating that the chips could have been damaged by too high voltage from one of the two low-voltage power supplies powering the chips of this station. The two power supplies were replaced in the experiment by spares and were thoroughly tested by the CERN electronics pool, but no problems were detected.

During the winter shutdown, several activities were performed in order to understand and fix the problem. All power cables of station 0 were tested, checking for bad connections, short circuits and pin swaps in the connectors. One cut sense wire was discovered close to a connector, along with missing grounding of the rack of station 0 and a patch panel located in this rack. The interlock board of station 0, responsible for shutting down low-voltage channels in case of overheating chips or a problem with the detector cooling plant, was inspected. The board was found to not function properly due to a fault in the Raspberry Pi connected to it. The fault was probably caused by a damaged microUSB cable used to power the Raspberry Pi. All found problems were addressed. A new crate and three low-voltage power supply modules (two powering the chips, one powering the PCB of a GTK module) were bought, tested by CERN electronics pool and finally installed in the rack of station 0, replacing the original crate and modules. It was further decided to install an older GTK module at station 0 as a matter of precaution.

The GTK has restarted the operation smoothly in 2024 with all the four stations working.

3.3 Other subsystems

Veto counter and CHANTI

The VetoCounter worked as expected in 2023 with the Felix readout in parallel to the TEL62. The restart of the operation in 2024 were smooth, with data for calibration taken during the muon run and used to adjust the high voltage settings of the photomultipliers.

Following the successful commissioning of the new TDC-Felix boards for the VetoCounter detector, the same readout system was adopted for the CHANTI detector, replacing the TEL62 boards. In total nine new TDCs with 390 ps digitization step were installed in the cavern, connected through the optical links to two Felix servers in the PC farm. Owing to the experience from VetoCounter, a boron shielding was placed around the TDC boards to minimize the damage from neutrons in the beam halo.

Other subdetectors

The STRAW detector and readout system were stable throughout the 2023 run, and the start of operation in 2024 has been smooth so far. One notable issue occurred in 2023 with an unexpected power cut in ECN3 resulting in a MPOD power supply crate failure.

The majority of the SiPMs of the NewCHOD have been replaced with new ones (type S14160). The connectivity of the channels has been reworked leading to a significant squeezing of the signals. Overall, the time resolution has improved and now is below 0.8 ns for all the channels.

The RICH and MUV3 worked smoothly in 2023, underwent ordinary maintenance during YETS and restarted properly in 2024.

No major interventions were done during YETS on the electromagnetic (LKr, LAV, IRC, SAC) and hadronic (MUV1, MUV2, HASC) calorimeters. All the detectors worked as expected in 2023 and restarted smoothly in 2024.

L0TP+, Trigger, PC farm

The L0TP+ board replaced the old L0TP since the beginning of the 2023 data taking. The commissioning of the new board lasted for the first three weeks of the run. In particular, a problem in the firmware was identified that was causing a high rate of bad events when the intensity exceeded 80% of the full intensity. The fix required a couple of weeks, during which the old L0TP was used to take data. The L0TP+ was then reinstalled after the June technical stop. A final debugging was performed during the run in dump when minor bugs were identified and fixed. A first look at the data processed online suggested slightly improved performance of the L0TP+ with respect to the L0TP in terms of dead time.

3.4 Plans for the 2024 run

In addition to the main kaon physics run, ten days of data in beam dump mode are scheduled in 2024, with the same beam and detector setup as that used in 2023. Another week of run at low intensity (about 2% of the full intensity) is planned, with the purpose to take data for precision measurements in the context of CKM studies.

The physics run has started on April 10. The steering of the beam was completed successfully the week before. The first two days of run were devoted to the Hydrogen filling, alignment, and pressure scan of the CEDAR-H, and to the calibration of the various sub-detectors. Presently, all the detectors are working as expected. The intensity is set to about $(20 \div 22) \times 10^{11}$ protons on target.

4 Data processing and quality

4.1 Data quality monitoring system

The quality of NA62 data relies on the online data quality monitoring system. This system is organised in three levels.

1. Fast Processing is meant to provide histograms in the Control Room and on the web for almost real-time monitoring. As soon as a spill is collected, a subset of data taken by a minimum bias trigger is processed using the standard offline reconstruction software. A dedicated PC dispatches the histograms. The time from taking data to displaying the histograms depends on the instantaneous intensity, and was about two minutes in 2023.

2. Fast Post-Processing; takes place at the end of a run, and provides a monitoring tool for detector experts on a daily basis, with larger statistics than the first level. This step makes use of the output files from the fast processing, therefore the delay time, typically few hours, depends only on the length of the run.

3. Prompt Processing relies on the offline processing of all the data from the raw files temporary stored on EOS. This level performs the full detector calibrations, filters the data and runs several analysis routines. The delay time is typically a few days, and is sensitive to possible configuration changes that may occur during data taking, halting the prompt processing of the whole run if not propagated to the software quickly enough.

During the 2023 run, more than 95% of the spills were fully processed by the prompt processing, which was a significant improvement with respect to previous data taking. Moreover, there was a sizable reduction of the Fast Processing time, thanks to a new system of receiving the data directly from the farm nodes instead of the merger PCs, and the improved spill quality.

The additional reduction in processing time foreseen by using a new reconstruction software in multi-thread mode was only partly successful due to the hardware limits of the cores in the monitoring PCs; nevertheless, a factor 2 was achieved.

For the 2024 data taking the full monitoring system is now running on AlmaLinux 9.

4.2 The 2023 data: reprocessing, statistics, quality

The 2023 data taking ended in September, and the offline central reprocessing is ongoing. The reprocessing software runs dedicated data-quality routines for each subsystem, to identify which spills are "bad" and must be excluded from the physics analyses. The full 2023 data sample is split into six *kaon mode* subsamples (A, B, C, D, E, F in chronological order) according to the main features of the data taking, and the *beam-dump mode* subsample; the data quality is almost uniform within each subsample. The 2023 data sample consists of 400×10^3 SPS spills in kaon mode, and 46×10^3 SPS spills in beam-dump mode.

According to the prompt processing, less than 10% of the collected spills in kaon mode are flagged as bad and excluded from the PNN analysis. This number is preliminary and should be confirmed at the end of the offline central reprocessing. The sources of bad spills are: issues in one or more subsystems used in the PNN analysis; the spills collected with trigger conditions not appropriate for the PNN analysis; or non-recoverable processing failures.

The PNN analysis has the largest fraction of bad bursts as it makes use of all the subdetectors. Some of the bad spills are usable in other physics analyses that do not rely on the information

coming from all subsystems. Studies to recover part of the bad spills for the PNN analysis are ongoing. No relevant remaining data quality issues are found for the data collected in 2023 and declared good for the PNN analysis.

5 Computing and Software

5.1 Computing requirements

A total of 2.5 PByte of raw data were written to CTA in 2023. Presently, the total amount of NA62 data on CTA (accumulated since 2012) is about 18.5 PBytes, of which 63% is raw data, and 35% is backup of processing output.

NA62 keeps a copy of the raw data in the CTA system at Rutherford Appleton Laboratory in the UK. RUN1 data were copied in 2021, and data taken in 2021–2023 were copied in early 2024. NA62 plans to copy the raw data of the upcoming data taking periods to RAL while they are still in the EOS buffer, avoiding the need to stage them back from CTA.

After processing and filtering, NA62 data are kept on EOS (and backup up on CTA) for individual user analyses. The projection made in 2020 based on 2018 data estimated a yearly increase of about 1 PByte. Due to the larger than expected size of the 2021 data, additional storage (2 PByte) was requested and granted in summer 2022. Additionally, the NA62 normal yearly allocation of 1.3 PByte was granted in March 2024. Presently, the total quota is 10.6 PByte, of which 200 TByte are reserved for online usage (raw data to CTA and prompt processing).

NA62 would like to express its gratitude to the IT Department for their support and expertise in assisting the needs of the experiment, and in particular to Xavier Espinal and Bernd Panzer-Steindel, for the excellent support and services provided.

5.2 Framework updates

The NA62 software framework has been fully migrated to `LCG_102b` during 2023. This migration was necessary due to the phase-out of the CentOS7 infrastructure.

Several event biasing schemes were introduced at the simulation level as part of the ongoing effort to understand the background mechanisms to the $K^+ \to \pi^+\nu\bar{\nu}$ decay. The decay generator library has been routinely developed to support the ongoing rare kaon decay analyses, the beam-dump programme and exploratory studies.

A new component, `na62jobs`, has been added to the NA62 software framework, with the purpose to standardize and automatize user jobs submission on the CERN batch system.

6 $K^+ \to \pi^+\nu\bar{\nu}$ analysis

Data collected in 2021 and 2022 is combined into a single unified dataset for the analysis. This dataset is comprised of 4.3×10^5 SPS spills passing all data quality checks. Events in the first second of SPS beam delivery (timestamp below 2 s) are removed for 2021 data because of degraded data quality due to spill conditions [5]; this corresponds to approximately 2% of the combined 21+22 dataset.

6.1 Selection overview & updates

Potential signal $K^+ \to \pi^+\nu\bar{\nu}$ decay candidates are selected using a stringent single-track selection exploiting all NA62 detector systems.

A K^+ is tagged by the KTAG and matched in time (within 0.5 ns) to a track reconstructed in the GTK. Events with additional activity in the GTK, which may arise due to pileup or decays in the upstream region, are rejected.

The reconstructed K^+ is then matched in time and space with a π^+ candidate track reconstructed downstream by the STRAW spectrometer, and identified as a π^+ using the RICH, calorimeters (LKr, MUV1, MUV2) and MUV3. The K^+–π^+ vertex must be within a fiducial volume (FV) with a length of 60 m (starting 6 m downstream of the final GTK station) and satisfying a set of momentum-dependent constraints on the angle of the π^+ track (using information about the vertex position and the radius at which the track reaches the first STRAW chamber). A new technique for matching the upstream K^+ and downstream π^+ candidate tracks is adopted for this analysis, using a bayesian likelihood to determine the quality of a given match and identify the possibility for an accidental match with a pileup GTK track. This new procedure maintains and slightly improves the matching performance of the RUN1-data analysis while being more flexible for adaptation to different conditions.

The downstream π^+ candidate track must have associated signals in the RICH, CHOD and LKr while remaining inside the geometric region defined by the active areas of these detectors and the MUV3. Precision timing for the downstream track is provided by the RICH and this must match both the KTAG and GTK track times within 0.5ns. The track is identified as a π^+ using the RICH ring and the energy deposits in the LKr and hadronic calorimeters (MUV1,2) and by the absence of an associated signal in the MUV3. The particle identification criteria have been re-optimised for the RUN2 dataset, and the boosted decision tree used to exploit calorimetric information has been re-trained with the new dataset.

A comprehensive set of veto criteria is then applied to ensure that there is no additional activity in the event. Photons are rejected using: the LKr, identifying any clusters not associated to the selected π^+ candidate track; 12 LAV stations, based on signals in stations downstream of the K^+–π^+ vertex; and small angle vetoes IRC and SAC, exploiting both of two parallel readout systems. The LKr photon veto time window has been significantly reduced, made possible due to an improved reconstruction. Additional charged tracks which may be associated to the selected track are rejected with 'multiplicity vetoes' using: extra signals in the CHOD and LKr not associated to the selected π^+ candidate track (with conditions overhauled and re-optimised for higher intensity RUN2 data); particle tracks fully or partially reconstructed by the STRAW which may form a vertex with the selected π^+ candidate track; the HASC, including the new station installed in 2021; and the MUV0. Events with decays in the upstream part of the beamline are detected using the VetoCounter, also installed in 2021; the ANTI0 is used to reject any tracks entering the FV from outside the beam pipe opening to the vacuum tube.

The updates to the analysis have increased the signal acceptance (at zero effective intensity) by 20% while maintaining performance and background rejection at the same level as for RUN1 data despite the higher intensities in RUN2. The effect of increased intensity for the analysis is presented in detail in section 2.3.

6.2 Signal sensitivity

The signal sensitivity is evaluated using the $K^+ \to \pi^+\pi^0$ decay for normalisation. The normalisation and signal selections are identical except that photon and multiplicity veto criteria are removed for the normalisation selection, and different kinematic selections based on the squared missing mass ($m^2_{miss} = (P_{K^+} - P_{\pi^+})^2$, the squared difference between the 4-momenta of the kaon and pion) are applied. The single event sensitivity, the branching ratio corresponding to the observation of one signal event, is given by

$$\mathcal{B}_{SES} = \frac{\mathcal{B}_{\pi\pi}}{D_0 N_{\pi\pi}} \frac{A_{\pi\pi}}{A_{\pi\nu\bar{\nu}}} \frac{1}{\varepsilon_{trig}\varepsilon_{RV}} \ , \tag{1}$$

where: $B_{\pi\pi}$ is the branching ratio of the $K^+ \to \pi^+\pi^0$ decay [6]; $A_{\pi\pi}$ and $A_{\pi\nu\bar{\nu}}$ are the normalisation and signal selection efficiencies, evaluated using MC with the SM model used for the signal), respectively; D_0 (generally 400) is the downscaling factor for the normalisation trigger and $N_{\pi\pi}$ is the number of normalisation events collected using this trigger; ε_{trig} is the effective trigger efficiency for collection of signal events; ε_{RV} is the 'random veto efficiency' which accounts for the probability of an event being rejected due to 'random' additional activity in coincidence with a signal candidate. Therefore, the number of expected SM signal events is given by

$$N^{\mathrm{SM,exp}}_{\pi\nu\bar{\nu}} = \frac{\mathcal{B}^{SM}_{\pi\nu\bar{\nu}}}{\mathcal{B}_{SES}} = \frac{\mathcal{B}^{SM}_{\pi\nu\bar{\nu}}}{\mathcal{B}_{\pi\pi}} \frac{A_{\pi\nu\bar{\nu}}}{A_{\pi\pi}} D_0 N_{\pi\pi} \varepsilon_{trig}\varepsilon_{RV} \ . \tag{2}$$

For the combined 21+22 dataset $N^{\mathrm{SM,exp}}_{\pi\nu\bar{\nu}} = 10.07 \pm 0.31$, with values summarised in table 2. The analysis is performed in independent categories defined in the interval $15 - 45\,\mathrm{GeV}/c$ divded into six $5\,\mathrm{GeV}/c$ momentum bins. Results for acceptances, trigger efficiencies and $N^{\mathrm{SM,exp}}_{\pi\nu\bar{\nu}}$ are shown for each category in figure 4. The random veto efficiency by definition is independent of the track momentum since it is related only to additional activity in the event. This additional activity however is dependent on the instantaneous beam intensity and therefore in figure 4 ε_{RV} is shown as a function of this variable.

The uncertainty on the single event sensitivity is improved significantly with respect to the RUN1 analysis, from 7% to less than 4%. This uncertainty is dominated by systematic effects and the improvement is primarily due to improved precision in the measurement of trigger efficiencies and a new higher-precision method for evaluation of the random veto efficiency.

Concurrently, the expected number of SM signal events per (good) burst has increased by 50% in 2022 with respect to 2018 data (with a smaller factor for the overall dataset due to the removal of part of the spill for 2021 data). This includes the effect of acceptance increase (at zero intensity) discussed above as well as the selection optimisations and improvements for higher efficiency at higher intensities (improved random veto efficiency), as well as additional statistics gathered at higher intensities.

6.3 Background evaluation

There are two classes of backgrounds: K^+ decays in the FV, and decays upstream of the FV.

The evaluation strategies for the first class of events is well-established and the same procedures as developed in the RUN1 analysis are used. Specifically, for the main decays $K^+ \to \pi^+\pi^0$, $K^+ \to \mu^+\nu$ and $K^+ \to \pi^+\pi^+\pi^-$, a data-driven procedure is employed: the number of events passing the full signal selection in an appropriate control region, N_{BR}, is scaled by a 'tail fraction' factor, f_{tail}. This factor is measured in an independent control sample and describes the probability

Table 2: Preliminary signal sensitivity for the combined 2021+22 dataset.

Variable	2021 ($t > 2$ s)	2022	21+22
$(N_{\pi\pi}D_0)/400$ $[\times 10^7]$	3.713	16.374	20.087
ε_{trig}	$(83.5 \pm 1.3)\%$	$(86.3 \pm 1.5)\%$	$(85.8 \pm 1.4)\%$
ε_{RV}	$(63.0 \pm 0.5)\%$	$(63.8 \pm 0.5)\%$	$(63.6 \pm 0.5)\%$
$A_{\pi\pi}$	$13.525 \pm 0.005\%$		
$A_{\pi\nu\bar{\nu}}$	$7.7 \pm 0.2\%$		
$\mathcal{B}_{SES}[\times 10^{-11}]$	4.68 ± 0.17	1.01 ± 0.03	0.83 ± 0.03
$N_{\pi\nu\bar{\nu}}^{\mathrm{SM,exp}}$	1.80 ± 0.06	8.28 ± 0.24	10.07 ± 0.31
$N_{\pi\nu\bar{\nu}}^{\mathrm{SM,exp}}$ per burst	1.7×10^{-5}	2.5×10^{-5}	2.3×10^{-5}

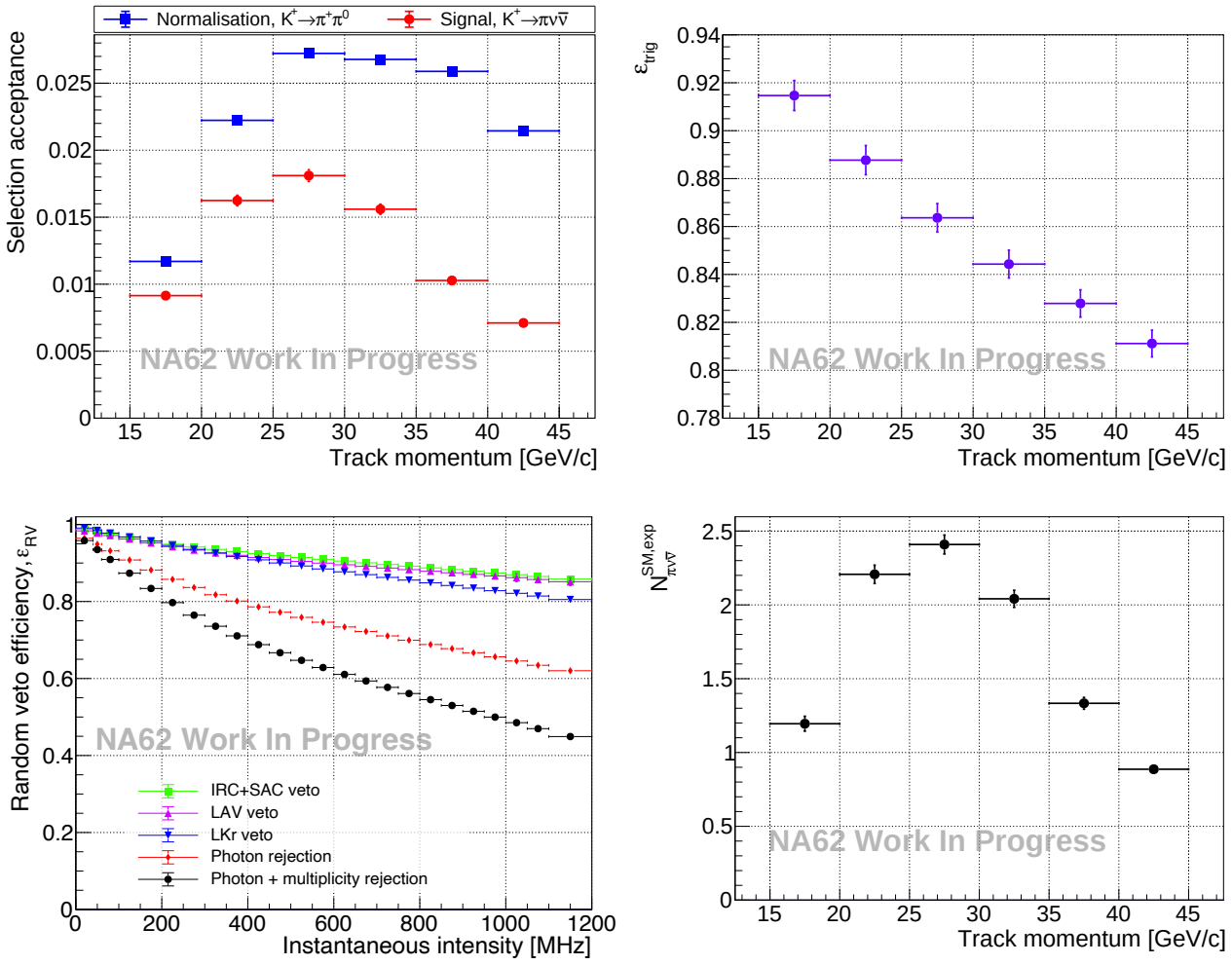

Figure 4: Upper left: signal (red) and normalisation (blue) selection acceptances in bins of track momentum. Upper right: relative trigger efficiency ε_{trig} as a function of track momentum. Lower left: random veto efficiency as a function of instantaneous beam intensity. Lower right: expected number of standard model signal events, assuming $\mathcal{B}(K^+ \to \pi^+\nu\bar{\nu}) = (8.4 \pm 1.0) \times 10^{-11}$ [7], in the 2021+2022 dataset.

of an event entering the signal region due to non-Gaussian tails (misreconstruction) in the m^2_{miss} kinematic variable with respect to the same control region. The background is therefore given by $N_{bg} = N_{BR} f_{tail}$. For the $K^+ \to \pi^+\pi^0 e^+\nu$ decay there is no appropriate side-band control sample dominated only by this process and therefore simulations are used to evaluate the background, scaling the number of selected MC events in the same way as for the single event sensitivity calculation. Background sources from other decays are effectively negligible and are also evaluated using MC simulations.

The strategy for evaluating the 'upstream' background follows the same principles as for the RUN1 analysis, but has been improved, becoming a fully data-driven procedure. The upstream background expectation is given by

$$N_{bg}^{ups} = \sum_i N_i f_{cda} P_i^{mistag} \ , \tag{3}$$

where: N_i is the number of events in a control sample with the full selection applied except the K^+–π^+ matching and requiring that the closest distance of approach between the K^+ and π^+ track is greater than 4 mm (inverting the standard condition); $f_{cda} = \frac{N(cda<4)}{N(cda>4)}$ is a scaling factor which quantifies the ratio of events expected with CDA less than or greater than 4 mm; and P^{mistag} is the probability for an event to pass the Bayesian K^+–π^+ matching discriminant conditions. The calculation exploits two variables as input to the Bayesian K+-pi+ matching discriminant: the GTK tracks and a time difference parameter, accounting for the difference between the GTK, KTAG and RICH signals. Bins (with index i) in a 2D distribution of these variables are considered. The control sample is the same as used for RUN1 analysis, however the evaluation of both f_{cda} and P^{mistag} has been updated. The factor f_{cda} is now evaluated directly from the same data used to count N, and P^{mistag} is measured, in each 2D bin i, from data as the fraction of $K^+ \to \pi^+\pi^0$ normalisation events passing the Bayesian K^+–π^+ matching discriminant criteria. The accuracy and precision of procedure is evaluated using ten validation samples, each defined by inverting at least one selection criteria used to reject upstream events and all mutually independent. These ten samples arise from five different selections with a pair of samples for each which require the m^2_{miss} either to be in the signal regions (odd numbered samples), or to have $m^2_{miss} < -0.05\,\mathrm{GeV}/c$ (which does not include any physical K^+ decays in the FV and are even numbered samples). In each of these validation samples the expectation and observation are found to be in good agreement, both as an integral across the six momentum-bin categories, as shown in figure 5, and in individual momentum categories.

The total upstream background expectation is found to have increased with respect to the RUN1 analysis. This is understood to be primarily due to the increased intensity and changes to the selection to improve signal yield. Nevertheless, investigations are ongoing to better understand the effect of intensity on this background and the comparison between RUN1 and RUN2 data. It is noted that the upstream background is reduced by a factor of approximately 2 using the new VetoCounter, making this an essential detector to maintain a reasonable background level at high intensities. The expected background is summarised in Table 3.

6.4 Summary

The first analysis of RUN2 data, using the combined 2021+2022 dataset, is almost complete. The signal yield has increased by 50% per (good) burst with respect to the RUN1 data analysis while maintaining the backgrounds from K^+ decays in the FV at the same level. The upstream background is now evaluated using a fully data-driven procedure and is found to be larger than

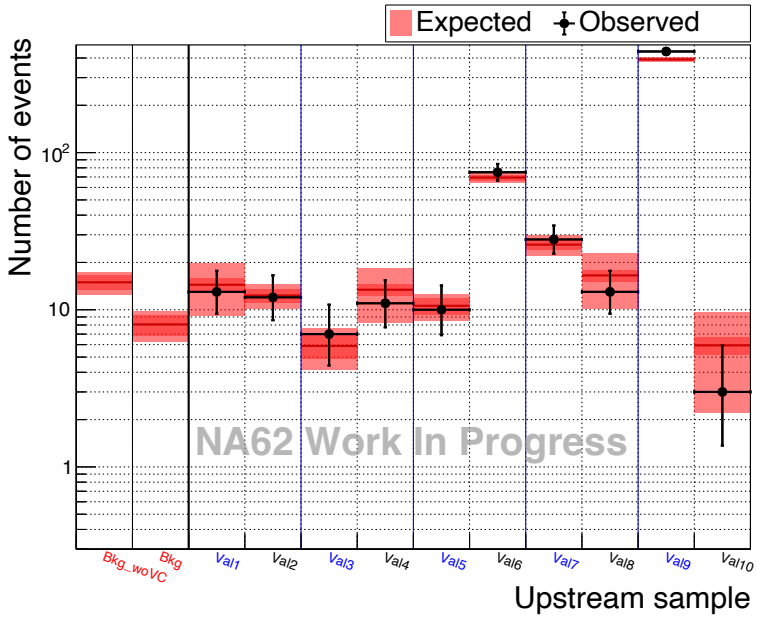

Figure 5: Expected (red) and observed (black) numbers of events in upstream validation samples. The first two bins do not show observations since these show the signal region without and with veto counter rejection applied, respectively.

Table 3: Preliminary number of expected background events for the 2021+2022 dataset. Results are presented for the sum of the two signal regions (R1+R2).

Process	N_{bg}
$K^+ \to \pi^+\pi^0(\gamma)$	0.86 ± 0.06
$K^+ \to \mu^+\nu(\gamma)$	0.93 ± 0.20
$K^+ \to \pi^+\pi^+\pi^-$	0.11 ± 0.03
$K^+ \to \pi^+\pi^-e^+\nu$	$0.84^{+0.35}_{-0.28}$
$K^+ \to \pi^0\ell^+\nu$	$< 10^{-3}$
$K^+ \to \pi^+\gamma\gamma$	0.01 ± 0.01
Upstream	$8.0^{+2.2}_{-1.8}$
Total background	$10.8^{+2.2}_{-1.9}$

initially expected. Nevertheless, taking into account both increases in signal and background, the overall sensitivity for the branching ratio measurement has been improved. This analysis includes a signal yield which is the same as the full RUN1 dataset, meaning the addition of this dataset doubles the total expected number of SM signal events with NA62 data.

Before presenting this result final checks and evaluations are ongoing to understand the differences between the RUN1 and RUN2 datasets, taken in significantly different conditions (in particular with regards the intensity). The analysis of the 2023 data, which includes lower (almost RUN1-like) intensity conditions, is an essential component of these studies and is underway.

7 Precision measurements of rare kaon decays

Prescaled multi-track and minimum-bias trigger lines, which have operated since the start of data collection in 2016 [8], enable a wide and active NA62 rare decay programme. A significant part of the programme is focused on K^+ decays to lepton pairs. The L0 trigger lines for collection of lepton pairs are based on RICH and CHOD multiplicity requirements, the total energy deposited in the LKr and MUV3 signal multiplicity conditions. The L1 trigger conditions involve beam kaon identification in the KTAG and reconstruction of a negatively charged track in the STRAW spectrometer. The RUN1 dataset is equivalent to 10^{12} kaon decays for the di-electrons triggers, 3×10^{12} decays for the di-muons, and 10^{12} decays for the electron-muon pairs trigger. The RUN1 dataset collected with generic multi-track and minimum-bias trigger conditions is equivalent to 10^{11} kaon decays. The size of the RUN2 rare-decay dataset collected so far already exceeds that of the RUN1 dataset, in part due to optimisation of the trigger algorithms and reduction of the prescaling factors.

Since the previous annual report to the SPSC, we published the first precision measurement of the $K^+ \to \pi^+\gamma\gamma$ decay based on 4.0×10^3 candidates selected from the RUN1 minimum-bias dataset [9]. We have established for the first time that the next-to-leading order (NLO) contribution in the Chiral Perturbation Theory (ChPT) is necessary to describe the observed di-photon mass spectrum. The decay branching ratio within the NLO ChPT modes is measured to be $(9.61 \pm 0.17) \times 10^{-7}$.

We published a precision measurement of the radiative $K^+ \to \pi^0 e^+ \nu\gamma$ decay based on 1.3×10^5 candidates (world's largest sample by far) selected from the RUN1 minimum-bias dataset [10]. The decay branching ratio is measured to a record percent-level precision, matching the precision of the ChPT calculation. An improved upper limit is set at a level below 10^{-2} on the possible T-violating asymmetry.

We presented a preliminary measurement of the rare decay $\pi^0 \to e^+e^-$ based on the RUN1 di-electron dataset at the Moriond EW conference in March 2024 [11]. For the first time, this measurement uses two-loop QED radiative corrections [12] and previously neglected contributions [13]. The measured decay branching ratio is $\mathcal{B}(\pi^0 \to e^+e^-(\gamma),\, m_{ee}^2/m_{\pi^0}^2 > 0.95) = (5.86 \pm 0.37) \times 10^{-8}$, compatible with the only previous measurement of similar precision [14] and in agreement with the SM expectation [15, 16]. A paper is in preparation.

A broad programme of searches for production of possible hidden-sector mediators in K^+ decays, and tests of lepton flavour and lepton number conservation in K^+ decays, is in progress. Since the previous annual report, we published the first search for the ultra-rare decay $K^+ \to \pi^+e^+e^+e^-e^-$, establishing an upper limit of 1.4×10^{-8} at 90% CL of the decay branching ratio, and the first search for pair-production of hidden-sector mediators in prompt cascades $K^+ \to \pi^+ aa$, $a \to e^+e^-$ and $K^+ \to \pi^+ S$, $S \to A'A'$, $A' \to e^+e^-$ [17]. We published the first search for

production and decay of an axion-like particle with gluon coupling in the process $K^+ \to \pi^+ a$, $a \to \gamma\gamma$ [9]. We used these results, along with those from searches for the $K^+ \to \pi^+ X_{\text{inv}}$ decay at NA62 [1, 18], to establish improved exclusion regions in the parameter space of the BC11 hidden-sector scenario [19, 20].

8 Neutrino tagging technique

Neutrino tagging [21–25] is a promising approach for accelerator based neutrino experiments. The method consists in associating a neutrino interaction with the meson decay (i.e. $\pi^\pm \to \mu^\pm \nu_\mu$ or $K^\pm \to \mu^\pm \nu_\mu$) in which the neutrino was originally produced. The properties of the neutrino can then be estimated kinematically from the decay incoming and outgoing charged particles. Such reconstruction allows to reach energy resolutions an order of magnitude better than with the conventional methods based on the neutrino interaction final states and is nearly free from energy scale uncertainties. In addition, the method allows to significantly reduce the systematics uncertainties on the initial neutrino flux.

The feasibility of this technique has been studied using the NA62 data taken in 2022 with a dedicated trigger line. The GTK and STRAW spectrometers allowed the reconstruction of the charged particles of the $K^+ \to \mu^+ \nu_\mu$ decay. The ν_μ interaction is detected as an in-time activity in the electromagnetic (LKr) and hadronic (MUV1, MUV2) calorimeters not associated to the muon track and consistent with the reconstructed neutrino kinematics. Two tagged-neutrino candidate events have been observed in a flux of about 1.5×10^{11} $K^+ \to \mu^+ \nu_\mu$ decays, in line with expectations. This constitutes the first experimental proof of principle of neutrino tagging, which NA62 has presented at the NuFact workshop in August 2023 [26]. A paper is in preparation.

9 Searches for exotic processes

At the time of writing, two data samples taken in beam-dump mode are available for analysis:

- data taken in October 2021: $(1.40 \pm 0.28) \times 10^{17}$ protons on dump;
- data taken in July 2023: $(2.39 \pm 0.48) \times 10^{17}$ protons on dump.[1]

In both cases, the currents of certain beamline magnets were adapted to optimise the sweeping of high-energy muons, as described in previous SPSC reports. The 2023 data was taken in part with the L0TP and in part with the L0TP+. This choice also allowed the full commissioning of the L0TP+.

Three analyses have been completed on the 2021 data-sample:

- A search for dark photons or axion-like particles decaying to $\mu^+\mu^-$ final states, published in JHEP [27].
- A search for dark photons decaying to e^+e^- final states, submitted to PRL [28], with a revised version produced after refereeing by the journal.

[1] This figure represents a conservative estimate on the uncertainty of the the integrated flux. Dedicated measurements have been done by the beam and RP division. Therefore a significant improvement on this number is expected.

- A search for dark photon, axion-like particle or dark scalar decays to hadronic final states, presented at Moriond QCD 2024 [29]. The final states probed were the following: 2π, 3π, 4π, $2K$, $2K\pi$, $2\pi\gamma$, $2\pi\eta$.

All above-mentioned analyses profit from a 'pointing approach': the total vertex momentum is extrapolated backwards to the point of closest approach to the nominal proton impact points on the TAX. As the signal is produced from proton interactions, it accumulates in a well-defined region in the plane of the distance of closest approach ($\mathrm{CDA_{TAX}}$) vs the longitudinal position of the minimum approach point ($\mathrm{Z_{TAX}}$). Signal and control regions, labelled as SR and CR, are defined and kept masked until the analysis blessing.

The background to the above analyses was determined through a mix of strategies, depending on the mechanisms producing it. To determine the halo-induced background, single muon tracks from an independent trigger line were backward-propagated to a plane preceding the decay-volume. This sample was used as an input to a GEANT4-based simulation, to compute muon-induced backgrounds and to predict the expected background in the SR/CR from this component. A dedicated simulation has been performed to evaluate the expected backgrounds from the interactions of neutrinos produced within the hadronic showers due to the dumped protons. This component proved to be negligible, at the present statistics, for any of the above analyses.

A background component was identified for the hadronic analysis, which had been irrelevant for the di-lepton searches performed so far. It stems from K^+ mesons that can pass the non-instrumented hole of the ANTI-0 detector. The presence of such K^+ mesons can be proved using the RICH detector. The K^+'s that decay before being identified in the RICH can undergo decays to hadronic final states, constituting a possible background component to this analysis.

Figure 6 shows the distribution of a control sample of data events with tracks not associated to ANTI0 in-time hits, mostly because originating in the ANTI0 hole, in the plane of Z_{VTX} vs the invariant mass of a $\pi^+\pi^-(\gamma)$ decay reconstructed in the fiducial volume (FV). Events with $K^+ \to \pi^+\pi^+\pi^-$ decays with one π^+ not reconstructed populate the FV for invariant masses below the K^+ mass. This K^+-induced background has been simulated using a selected single-track K^+ sample as a gun for the NA62 Monte Carlo simulation. The K^+ mesons are forced to decay as $K \to \pi^+\pi^+\pi^-$ in the FV. The expected background for all final states with hadrons is found to be below 0.04 events. In Figure 6, another component is visible, this time peaking around the K_S mass, due to $K_S \to \pi^+\pi^-$ decays. Missing a complete simulation of such component, a 3σ region around the K_S invariant mass has been masked for the preliminary analysis release.

The above-mentioned pointing strategy is straightforward for the di-lepton scenarios but more involved in the hadronic case: Signals with 'more complicated' topology (i.e. larger number of particles) can 'pollute' the SR of simpler topologies if one of the particles in the final state is not reconstructed. For example, a signal from a $2\pi\gamma$ final state could be reconstructed as a 2π final state if the photon is lost thus populating the correspondent SR/CR regions. For this reason, an appropriate unblinding strategy was chosen, starting from the CR/SR of more complicated topologies to the CR/SR of simpler topologies. After analysis blessing, all of the CR and SR of the probed final states were found to be empty and correspondingly a limit was set for the PBC benchmark cases BC4 and BC11, cf. Figure 7.

Two analyses are ongoing on the combined 2021+2023 dataset:

- a search for axion-like particles decaying to $\gamma\gamma$;
- a search for heavy neutral lepton decays to semileptonic channels and open decay channels involving neutrinos.

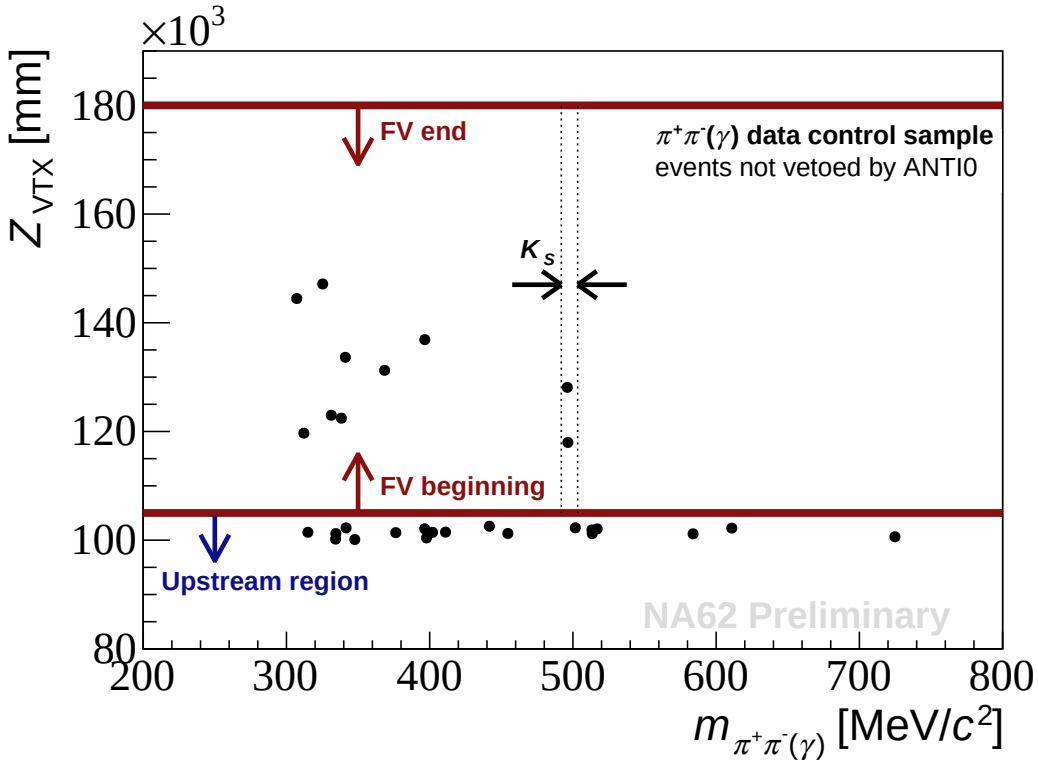

Figure 6: Events not in ANTI0 acceptance or not vetoed by ANTI0 in Z_{VTX} – invariant mass plane. Solid lines indicate the fiducial volume (FV). Dashed lines indicate the K_S 3σ mass window masked for the preliminary result.

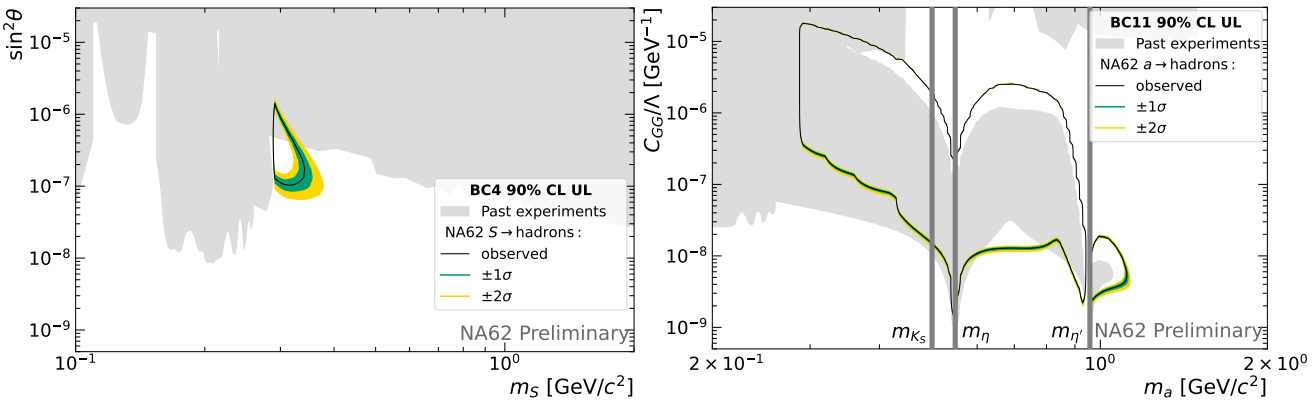

Figure 7: The observed 90% CL exclusion contours in BC4 (left) and BC11 (right) benchmarks together with the expected $\pm1\sigma$ and $\pm2\sigma$ bands (theory uncertainty not included). The public tool ALPINIST [30] is used for the combination of the results from the individual production and decay channels.

For the first case, a competitive search result can be expected with the recorded data samples. For the second one, we expect to use in the analysis the full envisaged beam-dump statistics by LS3 of 10^{18} protons dumped on the TAX.

10 Publications of NA62 data and older data

Since the last NA62 SPSC review in April 2023, the collaboration has completed the following publications:

- E. Cortina Gil et al. (NA62 collab.), Search for dark photon decays to $\mu^+\mu^-$ at NA62, Journal of High Energy Physics, Volume 2023, Issue 09, p.035 [27].
- E. Cortina Gil et al. (NA62 collab.), A study of the $K^+ \to \pi^0 e^+ \nu\gamma$ decay, Journal of High Energy Physics, Volume 2023, Issue 09, p.040 [10].
- E. Cortina Gil et al. (NA62 collab.), Improved calorimetric particle identification in NA62 using machine learning techniques, Journal of High Energy Physics, Volume 2023, Issue 11, p.138 [31].
- E. Cortina Gil et al. (NA62 collab.), Search for the K^+ decays into the $\pi^+ e^+ e^- e^+ e^-$ final state, Physics Letters B 846 (2023) 138193 [17].
- E. Cortina Gil et al. (NA62 collab.), Measurement of the $K^+ \to \pi^+\gamma\gamma$ decay, Physics Letters B 850 (2024) 138513 [9].
- E. Cortina Gil et al. (NA62 collab.), Search for leptonic decays of the dark photon at NA62, arXiv.2312.12055, submitted to Physical Review Letters [28].
- A. Bethani et al. (NA62 collab), Development of a new CEDAR for kaon identification at the NA62 experiment at CERN, arXiv.2312.17188, accepted by Journal of Instrumentation [4].

One more analysis, the very last one of the NA48/2 collaboration, based on the data recorded in 2003–2004, has been published:

- J. R. Batley et al. (NA48/2 collab.), First observation and study of the $K^\pm \to \pi^0\pi^0\mu^\pm\nu$ decay, Journal of High Energy Physics, Volume 2023, Issue 03, p.137 [32].

The collaboration is actively contributing to major international conferences and topical workshops with recently published or preliminary physics results from NA62 and NA48/2 data analyses. From May 2023 to April 2024, collaboration speakers presented 59 talks at international conferences of which 27 were invited talks, 37 were held in plenary, 22 in parallel sessions and 4 at Instrumentation Conferences. More contributions are already foreseen for the future 2024 conferences. Most notably, the highlights presented in the rare decays and in the exotic searches sections are presented at Moriond EW 2024 and Moriond QCD 2024 respectively.

References

[1] E. Cortina Gil et al. "Measurement of the very rare $K^+ \to \pi^+ \nu\overline{\nu}$ decay". In: *JHEP* 06 (2021), p. 093. DOI: 10.1007/JHEP06(2021)093. arXiv: 2103.15389 [hep-ex].

[2] CERN DG RB 2021 505.

[3] 2023 NA62 Status Report to the CERN, SPSC-SR-326.

[4] A. Bethani et al. "Development of a new CEDAR for kaon identification at the NA62 experiment at CERN". In: (Dec. 2023). arXiv: 2312.17188 [hep-ex].

[5] 2022 NA62 Status Report to the CERN, SPSC-SR-306.

[6] R. L. Workman et al. "Review of Particle Physics". In: *PTEP* 2022 (2022), p. 083C01. DOI: 10.1093/ptep/ptac097.

[7] A. J. Buras et al. "$K^+ \to \pi^+ \nu\overline{\nu}$ and $K_L \to \pi^0 \nu\overline{\nu}$ in the Standard Model: status and perspectives". In: *JHEP* 11 (2015), p. 033. DOI: 10.1007/JHEP11(2015)033. arXiv: 1503.02693 [hep-ph].

[8] E. Cortina Gil et al. "Performance of the NA62 trigger system". In: *JHEP* 03 (2023), p. 122. DOI: 10.1007/JHEP03(2023)122. arXiv: 2208.00897 [hep-ex].

[9] E. Cortina Gil et al. "Measurement of the $K^+ \to \pi^+ \gamma\gamma$ decay". In: *Phys. Lett. B* 850 (2024), p. 138513. DOI: 10.1016/j.physletb.2024.138513. arXiv: 2311.01837 [hep-ex].

[10] E. Cortina Gil et al. "A study of the $K^+ \to \pi^0 e^+ \nu\gamma$ decay". In: *JHEP* 09 (2023), p. 040. DOI: 10.1007/JHEP09(2023)040. arXiv: 2304.12271 [hep-ex].

[11] F. Brizioli (on behalf of NA62). "New results from analyses of rare kaon and pion decays at the NA62 experiment". https://indico.in2p3.fr/event/32664/contributions/137003/attachments/83684/124639/8_FBrizioli-v1.pdf.

[12] P. Vasko and J. Novotny. "Two-loop QED radiative corrections to the decay pi0 -> e+ e- : The virtual corrections and soft-photon bremsstrahlung". In: *JHEP* 10 (2011), p. 122. DOI: 10.1007/JHEP10(2011)122. arXiv: 1106.5956 [hep-ph].

[13] T. Husek, K. Kampf, and J. Novotny. "Radiative corrections to the Dalitz decay $\pi^0 \to e^+ e^- \gamma$ revisited". In: *Phys. Rev. D* 92.5 (2015), p. 054027. DOI: 10.1103/PhysRevD.92.054027. arXiv: 1504.06178 [hep-ph].

[14] E. Abouzaid et al. "Measurement of the Rare Decay $\pi^0 \to e^+ e^-$". In: *Phys. Rev. D* 75 (2007), p. 012004. DOI: 10.1103/PhysRevD.75.012004. arXiv: hep-ex/0610072.

[15] T. Husek and S. Leupold. "Two-hadron saturation for the pseudoscalar–vector–vector correlator and phenomenological applications". In: *Eur. Phys. J. C* 75.12 (2015), p. 586. DOI: 10.1140/epjc/s10052-015-3778-x. arXiv: 1507.00478 [hep-ph].

[16] M. Hoferichter et al. "Improved Standard-Model prediction for $\pi^0 \to e^+ e^-$". In: *Phys. Rev. Lett.* 128.17 (2022), p. 172004. DOI: 10.1103/PhysRevLett.128.172004. arXiv: 2105.04563 [hep-ph].

[17] E. Cortina Gil et al. "Search for K+ decays into the π+e+e−e+e− final state". In: *Phys. Lett. B* 846 (2023), p. 138193. DOI: 10.1016/j.physletb.2023.138193. arXiv: 2307.04579 [hep-ex].

[18] E. Cortina Gil et al. "Search for π^0 decays to invisible particles". In: *JHEP* 02 (2021), p. 201. DOI: 10.1007/JHEP02(2021)201. arXiv: 2010.07644 [hep-ex].

[19] J. Beacham et al. "Physics Beyond Colliders at CERN: Beyond the Standard Model Working Group Report". In: *J. Phys. G* 47.1 (2020), p. 010501. DOI: 10.1088/1361-6471/ab4cd2. arXiv: 1901.09966 [hep-ex].

[20] Y. Afik et al. "Probing long-lived axions at the KOTO experiment". In: *Phys. Rev. D* 108.5 (2023), p. 055007. DOI: 10.1103/PhysRevD.108.055007. arXiv: 2303.01521 [hep-ph].

[21] B. Pontecorvo. "Tagging direct neutrinos: a first step to neutrino tagging". In: *Lett. Nuovo Cim.* 25 (1979), pp. 257–259. DOI: 10.1007/BF02813638.

[22] I. P. Nedyalkov. *Single spectrometer station for neutrino tagging*. http://inis.jinr.ru/sl/NTBLIB/JINR-E1-84-515.pdf. July 1984. URL: http://inis.jinr.ru/sl/NTBLIB/JINR-E1-84-515.pdf.

[23] G. Bohm. *Project of a tagged neutrino facility at Serpukhov*. 1987.

[24] R. H. Bernstein et al. *A Proposal for a Neutrino Oscillation Experiment in a Tagged Neutrino Line*. 1990.

[25] M. Perrin-Terrin. "Neutrino tagging: a new tool for accelerator based neutrino experiments". In: *Eur. Phys. J. C* 82.5 (2022), p. 465. DOI: 10.1140/epjc/s10052-022-10397-8. arXiv: 2112.12848 [hep-ex].

[26] B. De Martino (on behalf of NA62). "Experimental proof of principle of the Neutrino Tagging technique at NA62". https://indico.cern.ch/event/1216905/contributions/5448754/attachments/2702123/4690877/NuFACT_NuTagging_DeMartino.pdf.

[27] E. Cortina Gil et al. "Search for dark photon decays to $\mu^+\mu^-$ at NA62". In: *JHEP* 09 (2023), p. 035. DOI: 10.1007/JHEP09(2023)035. arXiv: 2303.08666 [hep-ex].

[28] E. Cortina Gil et al. "Search for leptonic decays of the dark photon at NA62". In: (Dec. 2023). arXiv: 2312.12055 [hep-ex].

[29] J. Jerhot (on behalf of NA62). "First NA62 search for long-lived new physics particle hadronic decays". https://moriond.in2p3.fr/QCD/2024/FridayMorning/Jerhot.pdf.

[30] J. Jerhot et al. "ALPINIST: Axion-Like Particles In Numerous Interactions Simulated and Tabulated". In: *JHEP* 07 (2022), p. 094. DOI: 10.1007/JHEP07(2022)094. arXiv: 2201.05170 [hep-ph].

[31] E. Cortina Gil et al. "Improved calorimetric particle identification in NA62 using machine learning techniques". In: *JHEP* 11 (2023), p. 138. DOI: 10.1007/JHEP11(2023)138. arXiv: 2304.10580 [hep-ex].

[32] J. R. Batley et al. "First observation and study of the $K^\pm \to \pi^0\pi^0\mu^\pm\nu$ decay". In: *JHEP* 03 (2024), p. 137. DOI: 10.1007/JHEP03(2024)137. arXiv: 2310.20295 [hep-ex].